Topics in Catalysis Vol. 44, Nos. 1–2, June 2007 (© 2007)
DOI: 10.1007/s11244-007-0295-7

Ceria-zirconia supported Au as highly active low temperature Water-gas shift catalysts

A. Amieiro Fonseca[a], J. M. Fisher[a], D. Ozkaya[a], M. D. Shannon[b,c], and D. Thompsett[a,*]

[a]*Johnson Matthey Technology Centre, Blounts Court, Sonning Common, Reading, RG4 9NH, UK*
[b]*ICI Measurement Science Group, Wilton Centre, Redcar, Cleveland, TS10 4RF, UK and on part-time secondment at* [c]*UK SuperSTEM Facility, CLRC Daresbury Laboratories, Leckwick Lane, Warrington, WA4 4AD, UK*

$Au/CeZrO_4$ catalysts have shown very low temperature activity for the WGS reaction. Characterisation of the as-prepared catalysts shows Au is present primarily as isolated Au^{3+} atoms. It has been found that a higher proportion of Au^{3+} present in the as-prepared catalyst leads to a higher WGS activity, although under reaction conditions reduction to Au^0 is observed. Use of TPR and iso-thermal H_2O re-oxidation has shown that Au reacts with H_2O at lower temperatures than an equivalent $Pt/CeZrO_4$ catalyst, indicating that H_2O activation is key in the onset of low temperature WGS activity.

KEY WORDS: Water-gas shift; Au; cerium–zirconium mixed oxides; TEM; XPS; TPR; Mechanism.

1. Introduction

The recent rapid development of low temperature fuel cell technology, in particularly the Polymer Electrolyte Fuel Cell (PEFC), has triggered a corresponding increase of research into small-scale hydrogen generation and purification [1]. In recent years, much emphasis has been placed on the identification and development of CO removal catalysts as conventional PEFC anode catalysts such as PtRu alloys that can only tolerate ppm levels of CO in H_2 reformate [2]. Therefore, PEFC compatible fuel processors require an extensive CO removal system consisting of a number of water-gas shift (WGS) and preferential oxidation (PROX) reactors to reduce the reformate CO content from % to ppm levels. However, recent advances in the PEFC area, both in the design of more CO tolerant anode catalysts such as PtMo alloys and in advanced proton conducting membranes that can operate at higher temperatures, suggest that future PEFCs systems could tolerate much higher levels of CO than can be at present [3,4]. Indeed, the use of H_3PO_4 doped Poly(benzimidazole) (PBI) based membranes allow operation at temperatures above 150 °C and have been shown to tolerate reformate CO concentrations of *c*. 1% CO, thus lessening the need for such extensive CO clean-up systems [5].

The WGS is a key process in the purification of hydrogen from syn-gas and reformate feeds. Current industrial processes utilise both a high temperature shift (HTS) catalyst (typically Cr doped Fe_2O_3) and a low temperature shift (LTS) catalyst ($Cu/ZnO/Al_2O_3$) that together take advantage of the higher reaction kinetics at high temperature and the shift of the equilibrium to lower CO concentrations at lower temperatures. Typically LTS catalysts achieve equilibrium conversion at *c*. 200 °C reducing CO concentrations to 0.2% (i.e. 2000 ppm). This may be still too high for PEFCs operating at *c*. 100 °C, and therefore, the development of lower temperature WGS catalysts would be attractive, as this would lower CO levels further due to higher equilibrium conversions and thus limit the need for PROX. In addition to low temperature activity, WGS catalysts for PEFCs would also need to be tolerant to start-up and shut-down procedures involving purging with air [1]. Conventional $Cu/ZnO/Al_2O_3$ catalysts are known to be pyrophoric on exposure to air after reduction, although a recent report suggests this limitation can be overcome [6].

The use of supported Au catalysts have widely been reported for the low temperature oxidation of CO in air and more recently for the low temperature oxidation of CO by H_2O (WGS). The first report by Andreeva *et al.* in 1996 demonstrated that a $Au/\alpha\text{-}Fe_2O_3$ catalyst showed higher activity than $Cu/ZnO/Al_2O_3$ below 200 °C under simple WGS conditions [7,8]. This catalyst was found to have poor stability even at moderate temperatures under WGS feeds due to the instability of the Fe_2O_3 under reducing conditions [9]. This initial report was followed by Sakaurai *et al.* who showed that Au/TiO_2 had significantly better WGS activity than $Cu/ZnO/Al_2O_3$ [10]. This work itself was inspired by earlier work that showed that Au catalysts had significant CO and CO_2 hydrogenation activity and hence Reverse-Water-Gas-Shift activity [11]. More recent work has shown that Au supported on a range of supports such as TiO_2 [12–14], ZrO_2 [15,16], ZnO [15], Na-ZSM5 and Na-mordernite [17] all have significant WGS activity. In

* To whom correspondence should be addressed.
E-mail: thompd@matthey.com

particular, it has been found that CeO_2 [18–20] and mixed oxides containing CeO_2 (e.g. La–CeO_2, Gd–CeO_2 [21,22], $(Na_{0.33}Ce_{0.66})_2Ti_2O_7$ [23]) show better activity and stability than other Au supported catalysts.

Much has been discussed on the nature of the active species under WGS conditions with surface atoms of small Au nanoparticles [24,25], atoms at the interface between particles and support [26,27] and cationic Au atoms all being proposed as the active sites for WGS [20,22]. In particular, Fu et al showed that taking an active Au/La–CeO_2 catalyst and leaching it with NaCN which reduced the Au loading by 90% did not change the WGS activity [20,21]. This indicated that a high proportion of the initially deposited Au was spectator to the overall reaction. Characterisation of the leached catalyst showed that Au was only present as ionic Au species and it was these species that were proposed as being active under WGS conditions. However, very recent *in-situ* X-ray absorption measurements have suggested that only small reduced Au clusters are present under WGS reaction conditions [25, 28].

In addition to the nature of the active site(s), there has been a vigorous discussion on the mechanism that Au catalysts show for WGS, as part of a wider discussion on the mode of operation of precious metal WGS catalysts. Two general mechanisms have been proposed; a regenerative (''redox'') mechanism based on the reduction of the catalyst (support) by CO to release CO_2 and subsequent re-oxidation by H_2O to release H_2, and an associative (''formate'' or ''carboxylate'') mechanism where CO reacts with bound OH groups forming carboxylate species (e.g. formate or carbonate) which then react with H_2O to give CO_2 and H_2. The use of *operando* diffuse-reflectance infrared Fourier transport spectroscopy (DRIFTS) combined with mass spectroscopy (MS) has been extensively used to elucidate the reaction mechanism over Au WGS catalysts (and other metal promoted CeO_2 catalysts) [27,29,30]. However, no clear agreement has been reached over the prime mechanistic pathways perhaps due to the study of different catalysts under different reaction conditions. Indeed, very recently Burch has proposed an 'universal' WGS mechanism which includes elements of both the regenerative and associative mechanisms which vary depending on the reaction conditions [31].

Given that the most active and stable catalysts are on support materials, such as CeO_2, that show redox properties, this suggests that oxides that have been developed which maximise both ease of redox behaviour and the stability over extended reduction/oxidising cycles may be useful as WGS supports. One such class of oxides are the ceria-zirconia mixed oxides developed primarily for gasoline automotive exhaust catalysts. The addition of Zr to the ceria lattice has been shown to have a significant effect on both oxygen storage capacity and stability of this OSC. The Zr allows the storage and release of oxygen from not just surface layers as with pure CeO_2 but from the bulk lattice structure [32,33].

This paper reports the use of a $CeZrO_4$ mixed oxide as a support for Au suitable for low temperature WGS; the effect of Au loading on WGS activity; characterisation and discussion on the nature of the Au speciation of the as prepared catalyst and under reactive conditions; the origin of the particularly low temperature activity of Au/$CeZrO_4$, and the stability of this activity to typical WGS feeds.

2. Experimental

2.1. Materials

CeO_2 and $CeZrO_4$ (50:50 atomic ratio) (Surface Areas 250 and 100 m^2g^{-1}, respectively) were obtained from Rhodia. ZrO_2 was obtained from MEL (SA 55 m^2g^{-1}). TiO_2 (P25, SA 55 m^2g^{-1}) was obtained from Degussa. All supports were calcined at 500 °C for 2 h before use. $HAuCl_4$ and Pt nitrate solution (15.7 wt% Pt) were Johnson Matthey products.

2.2. Catalyst preparation

2.2.1. Au/$CeZrO_4$

Au was deposited onto supports using a modification of the hydrolysis/precipitation method [34]. A typical preparation is given below for a 2 wt%Au/CeZrO4 catalyst.

$CeZrO_4$ support (pre-fired at 500 °C in air for 2 h) (19.6 g) was slurried in H_2O (800 cm^3) and heated to 60 °C. The pH was adjusted to 8.0 by the addition of Na_2CO_3 (0.05 M). $HAuCl_4$ (0.81 g, 49.2 wt%Au) was dissolved in H_2O (150 cm^3) and pumped into the stirred slurry at c. 10 cm^3min^{-1}. The pH was monitored throughout and extra Na_2CO_3 solution was pumped at a variable rate to maintain the pH as close as possible to 8.0 throughout the Au addition. This was achieved using a 3-term P.I.D. controller with feedback loop to the pH probe. On complete Au addition, the slurry was stirred a further 1 h, then filtered, washed thoroughly with H_2O to remove chloride and dried at 105 °C for 16 h in air. Au deposition was not quantitative especially at Au loadings above 2 wt%.

2.2.2. '4'%Au/'FeO(OH)'

$HAuCl_4$ (2.1 g, 49.4 wt%Au) and $Fe(NO_3)_6.9H_2O$ (126.45 g, Aldrich) were dissolved in H_2O and the total volume made up to 200 cm^3. The resulting solution was poured rapidly into a stirred aqueous Na_2CO_3 solution (106 g in 1.5 l). After stirring for 5 h at ambient temperature, the resulting precipitate was filtered, washed with H_2O and dried at 100 °C for 12 h. The resulting Au content by ICP was 1.5 wt%, indicating only 38% of Au was deposited.

2.2.3. 4wt%Pt/$CeZrO_4$

$CeZrO_4$ support (24 g) was slurried in H_2O (80 cm^3). Pt nitrate solution (6.37 g, 15.7% Pt) was diluted to 20 cm^3 and added to the slurry at room temperature. After 2 h stirring, no Pt remained in solution and the slurry was filtered, washed to remove nitrate ions, dried at 105 °C for 16 h and calcined at 500 °C for 2 h in air.

2.3. Characterisation

2.3.1. Assay

Samples were fused with Na_2O_2 in ZrO_2 crucibles. On cooling, the residue was dissolved in acidic H_2O and analysed using ICP.

2.3.2. XRD

XRD patterns were measured on a Bruker AXS D-500 instrument. Radiation with Cu Kα (Ni filtered) with a LaB6 (NIST SRM 660) line profile standard. Profile fitting (Topas P V1.01, Bruker-AXS) was necessary to deconvulute all peaks.

2.3.3. XPS

X-ray photoelectron spectra were measured on a VG ESCALAB 250 instrument. Samples were mounted on the specimen stage using double-sided adhesive tape and analysed with monochromatic Al Kα radiation in a 500 μm spot at 150W power. An in-lens flood gun was used for charge neutralisation and the binding energies were references to C 1s at 284.8 eV.

2.3.4. TEM

A small amount of sample was dusted onto a holey carbon copper grid. The samples were examined with a Tecnai F20 Transmission Electron Microscope using the following instrumental conditions; 200 kV voltage and 30 & 50 m C2 aperture. Both bright field and scanning TEM (high angle annular dark field (HAADF) methods were used together with Energy Dispersive X-ray spectroscopy (EDX).

2.3.5. SuperSTEM

Powder samples were crushed between two glass slides and a holey carbon copper TEM grid was dusted with the sample. The samples were examined in the SuperSTEM facility at Daresbury using 100 kV with Cs correction (Nion type). Both bright field high-resolution electron microscopy and high angle annular dark field (HAADF) methods were used to examine the samples.

2.3.6. Catalyst activity testing

Catalysts were tested in a glass micro-reactor held within a furnace. The furnace and surrounding pipe work was contained within an oven set at 110 °C to prevent water condensation. Gases were supplied via mass flow controllers and water was pumped into a steam pot via a calibrated peristaltic pump. A four-way valve arrangement enabled either inlet or outlet gas samples to be sent to the analyser (Maihak, CO, CO_2 analysis by IR, H_2 analysis by TCD). Catalyst samples were pelletised and sieved to give 250–355 μm particles prior to testing and placed in a glass micro-reactor with quartz wool at each end. Thermocouples were placed at the inlet, oulet and in the catalyst bed. Water-gas shift testing used a 30% H_2O, 5% CO, balance N_2 feed at a space velocity of 40,000 $cm^3g^{-1}hr^{-1}$. In a typical test, the catalyst charge was 0.45 g and the total flow was 300 cm^3min^{-1}.

The apparent turn-over frequencies (s^{-1}) were calculated by dividing the CO reaction rate (in terms of mmol s^{-1} CO reacted) by the number of Au sites (mmol) available, assuming all the Au is active.

2.3.7. Temperature programmed and isothermal experiments

H_2 TPR runs were performed in a micro-reactor with katharometer gas detection (ramp at 10 °C min^{-1} with 10% H_2/N_2 (30 cm^3 min^{-1}).

CO TPR runs were in the same micro-reactor (ramp at 5 °C min^{-1} with 7%CO/N_2)

Isothermal H_2O oxidations were performed in the micro-reactor using a Maihak analyser to monitor CO, CO_2 and H_2. In a typical experiment 1 g of sample was treated as follows;

The sample was heated to 200 °C in 13.3% H_2/N_2 (300 cm^3 min^{-1}) at 5 °C min^{-1}. It was then held at 200 °C and N_2 was flushed (300 cm^3 min^{-1}) to remove all H_2. Then a flow of H_2O (80 cm^3 min^{-1}) and N_2 (200 cm^3 min^{-1}) was introduced. After complete reaction, the sample was cooled to ambient in N_2 (200 cm^3 min^{-1}). The sample was then further heated to 350 °C in 13.3% H_2/N_2 (300 cm^3 min^{-1}) at 5 °C min^{-1} and H_2O/N_2 was introduced as above.

Cycled experiments were performed as above. In a typical experiment 1 g of sample was treated as follows;

The sample was heated to 220 °C in 7%CO/N_2 (300 cm^3 min^{-1}) at 5 °C min^{-1}. It was then flushed with N_2 isothermally, followed by 30% H_2O/N_2 (flow rate 300 cm^3 min^{-1}) until complete reaction. The sample was further flushed with N_2, followed by 7%CO/N_2 and repeat.

3. Results & discussion

3.1. Effect of support on Au WGS activity

To investigate the effect of support on Au WGS activity, a series of 2 wt%Au catalysts were prepared by a modified hydrolysis precipitation method using $HAuCl_4$ as a precursor onto commercially available CeO_2, TiO_2 and ZrO_2 supports. In addition, a series of Au/FeO_x catalysts were prepared, as Au/Fe_2O_3 catalysts had been reported to show good low temperature WGS activity. Au was deposited onto amorphous $FeO(OH)$,

crystalline α-Fe_2O_3, γ-Fe_2O_3 and Fe_3O_4 by hydrolysis/precipitation. In addition a further catalyst was prepared via co-precipitation with Au^{3+} and Fe^{3+} to give an XRD amorphous Au/'FeO(OH)' material. Of these catalysts, the co-precipitated catalyst gave the lowest temperature activity and was studied further. The catalysts were tested using a simple WGS mixture of 5%CO, 30% H_2O, balance N_2. Figure 1 shows the WGS activity as CO conversion for the first temperature ramp of the Au/CeO_2, TiO_2, ZrO_2 and Au/'FeO(OH)' samples. All 4 catalysts have onset temperatures of 100–110 °C, although the Au/'FeO(OH)' catalyst shows a more rapid rise in conversion, reaching maximum conversion at 170 °C. However, on the subsequent temperature ramp down, the catalyst showed rapid deactivation that appeared to be associated with collapse of catalyst surface area caused by reduction. In addition, TEM images of the tested catalyst showed the presence of discrete Au particles (2–6 nm) that were absent in the as prepared catalyst. Of the other catalysts, the Au/TiO_2 and ZrO_2 catalysts had similar activity profiles, reaching maximum conversion at *c.* 300 °C. It is interesting to note that these two supports would not be expected to show bulk redox properties. The Au/CeO_2 catalyst had the lowest activity, with maximum CO conversion occurring above 300 °C. The temperature ramps were found to be stable as long as the maximum temperature did not exceed 300 °C.

Although, the low temperature WGS activity of Au supported TiO_2 and CeO_2 catalysts have been widely reported, the good activity of the Au/ZrO_2 catalyst was relatively unexpected although there has been two recent reports showing similar activity of Au/ZrO_2 catalysts to Au/TiO_2 and Au/Fe_2O_3 catalysts [15,16] Given that the addition of ZrO_2 enhances the activity and stability of CeO_2 based catalysts [28,29], the activity of Au supported on a commercial 50:50 mole ratio $CeZrO_4$ material was investigated. Interestingly, it gave the lowest temperature WGS activity of the tested catalysts, with significant CO conversion at 100 °C and full conversion by 200 °C.

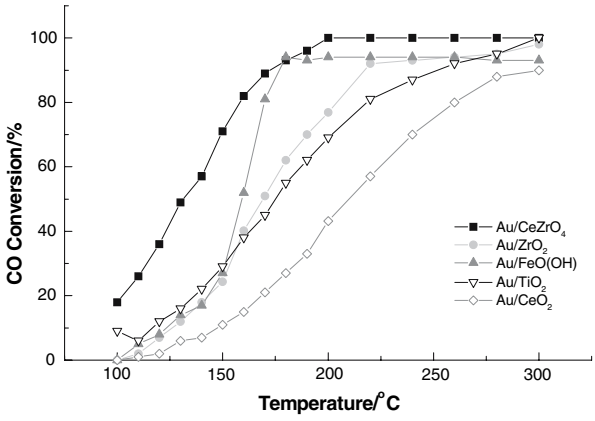

Figure 1. WGS activity as a function of temperature for a series of 2 wt% Au catalysts on a range of supports (5% CO, 30% H_2O, 65% N_2, 40,000 $cm^2g^{-1}h^{-1}$).

3.2. Effect of Au loading

To investigate the use of $CeZrO_4$ as a support for Au further, a series of catalysts with different Au loadings were prepared at nominally 0.2, 1, 2 and 4 wt%. In practise the actual Au loadings obtained were 0.19, 0.87, 1.70 and 2.99 wt%, respectively, indicating the effectiveness of Au deposition declines with loading especially above 2wt%. The CO conversion of the first temperature ramps is shown in figure 2. This data was used to calculate the conversion rate ($mmols^{-1}g^{-1}{}_{CAT}$) and the apparent turn-over-frequency (tof, s^{-1}) (assuming all the Au present was active).

Figure 3 shows the CO conversion and tof at 125 °C for the 4 catalysts. The CO conversion was found to increase with Au loading reaching a plateau at 1.70 wt%, after which no further increase in activity was found. In contrast, the highest tof was shown by the 0.19 wt%Au catalyst, and tof decreased with increasing loading. These results suggest that at the lowest loading, a maximum proportion of Au active sites (of the total Au present) for WGS exist. On increasing the Au loading, although the CO conversion rate increases indicating an increase in active sites, this is outweighed by a greater increase in Au "spectator" (or less active) species concentration. Assuming that at 0.19 wt%Au, 100% of Au species are active, by 1.70 wt% only c. 50% of the Au present are these similarly active species, thus showing a 50% drop in tof. Increasing the Au loading to 2.99 wt%, no further increase in conversion is observed indicating no further increase in active Au species concentration, but a further 50% increase in Au "spectator" species.

Figure 4 shows the Ln of the CO conversion rate as a function of 1/T. All 4 catalysts give reasonable linear fits at low CO conversion and show similar apparent activation energies (*c.* 28 kJ mol^{-1}), indicating similar rate determining steps. This is somewhat lower than values that have been reported for Au/CeO_2 (*c.* 40 kJ mol^{-1}), possibly due to the role of $CeZrO_4$ in promoting the WGS reaction with Au.

3.3. Au catalyst characterisation

The 1.70 wt% $Au/CeZrO_4$ catalyst was examined using powder X-ray Diffraction (XRD) to determine whether crystalline Au particles were present and if so, what size. Figure 5 shows the XRD of the as-prepared 1.70 wt%Au catalyst. The diffraction pattern of the crystalline $CeZrO_4$ is clear which is assignable to a tetragonal structure, however, there is no evidence of Au crystallites even after background subtraction, suggesting that if the Au present is crystalline then it is at sizes less than 2 nm.

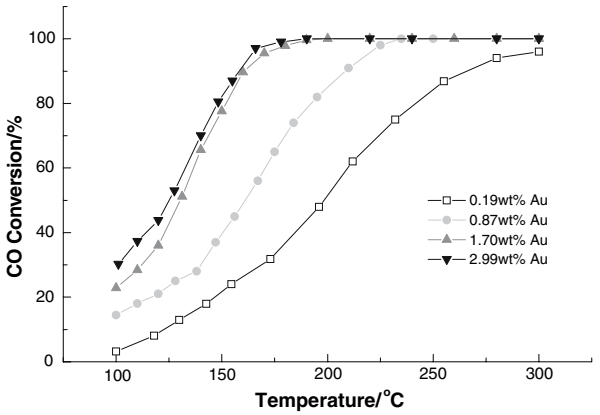

Figure 2. WGS activity (CO conversion) as a function of temperature for a series of Au/$CeZrO_4$ catalysts (5% CO, 30% H_2O, 65% N_2, 40,000 $cm^2g^{-1}h^{-1}$).

The 0.19, 0.87 and 1.70wt% Au catalysts were examined by XPS. Figure 6 shows the Au (4f) region of the XP spectrum of as-prepared 0.19 and 1.70 wt% Au/$CeZrO_4$ catalysts and table 1 shows the peak energies, atomic concentration and relative concentration after deconvolution. In all 3 catalysts, the measured atomic concentration of Au is high compared to the assayed value (0.13 at%–0.19 wt%, 1.28 at%–0.87 wt%, 2.61 at%–1.70 wt%) suggesting that the Au is at the surface of the catalyst and highly dispersed.

Although, the signal-to-noise for the spectrum of the 0.19 wt% Au catalyst is poor, the peaks can be predominately fitted to one Au species at a $4f_{7/2}$ binding energy of 87.3 eV. As the Au loading increases, the Au(4f) profile becomes more complex with deconvolution suggesting with the 0.87 wt% catalyst two species ($Au4f_{7/2}$ BE's 86.7 and 85.4 eV) are present and the 1.70 wt% catalyst shows three species (86.5, 85.3 and 83.9 eV). With reference to literature values, the peaks between 87.3 and 86.5 eV can be assigned to Au^{3+}, those at 85.4 and 85.3 eV to Au^+ and that at 83.9 eV to Au^0 [35]. Therefore, at low loadings the Au in the as-prepared catalysts appears present as exclusively Au^{3+}. As the Au loading increases firstly Au^+ and finally Au^0 species appear, however, even at 1.70 wt% the majority of Au is still present as Au^{3+}.

The assignment of XPS spectra of nanoparticle Au catalysts is somewhat controversial. In particular, the assignment of Au^+ species has also been explained as Au^0 species subjected to final state effects at small particle sizes, especially when supported on insulating supports [36–38]. In contrast, recent ^{197}Au Mössbauer studies have indicated that nanoparticle Au catalysts can contain discrete Au^+ species, which are presumably partially oxidised Au atoms at the surface of the small Au particles [39].

The 0.19 and 1.70 wt% as prepared Au/$CeZrO_4$ samples were examined using the SUPERSTEM instrument at Daresbury using both aberration corrected (0.11 nm resolution) high angle annular dark field (HAADF) and bright field STEM images. HAADF images of the 1.70 wt% Au sample appeared to show two types of Au containing features (as shown in figures 7a and 8) as characterised by high contrast features. A bright field STEM image of the same region is shown in figure 7b. In contrast, no similar features that could be ascribed to Au could be easily discerned, so HAADF images were preferred for this investigation. The SuperSTEM instrument used was not equipped with EDAX analysis, rendering direct atomic recognition not possible. However, Electron Energy Loss Spectroscopy (EELS) was used in an attempt to equivocally determine the Au composition of the high contrast features, but due to the Au $M_{4/5}$ edges being *c.* 2200 eV with wide edge shapes and low jump ratios coupled with relatively low Au sample concentrations, no discernable peaks were observed.

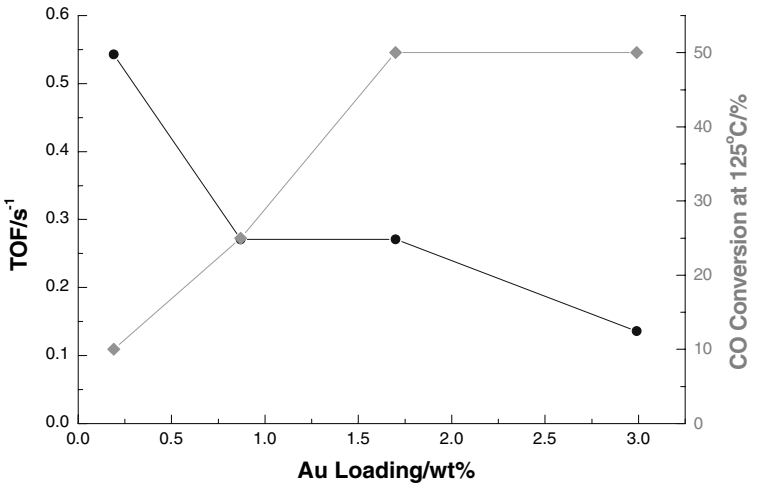

Figure 3. WGS activity as turn-over-frequency and CO conversion at 125 °C for the series of increasingly loaded Au/$CeZrO_4$ catalysts (5% CO, 30% H_2O, 65% N_2, 40,000 $cm^2g^{-1}h^{-1}$).

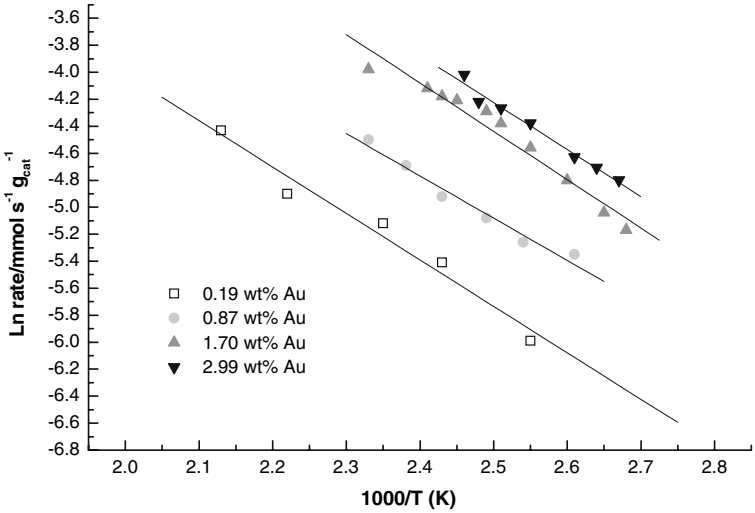

Figure 4. WGS activity (rate of CO conversion) as a function of temperature for a series of $Au/CeZrO_4$ catalysts (5% CO, 30% H_2O, 65% N_2, 40,000 $cm^2g^{-1}h^{-1}$).

The HAADF image of the 1.70 wt% Au sample showed two types of high contrast feature (figures 7a and 8b & c); patches typically *c*. 1 nm in diameter and very small features *c*. 0.3 nm in diameter. Images of the 0.19 wt% Au sample (not shown here) only showed the 0.3 nm features.

We interpret the *c*. 1 nm features to be metallic Au clusters and the *c*. 0.3 nm features to be individual Au (metallic?) atoms. The assignment of these latter features as individual Au atoms is supported by line intensity profiles. Figure 8a shows a line intensity profile across a 3 nm portion of the sample that does not contain any 0.3 nm features. The underlying intensity decreases from left to right indicating that the thickness of the sample is decreasing in a linear manner. Superimposed on this background are the individual variations of the CeZr lattice columns. Figure 8b shows the same region after a further 3 min on exposure to the electron beam. There is now superimposed on the underlying CeZr lattice, one possibly two features with twice the expected intensity.

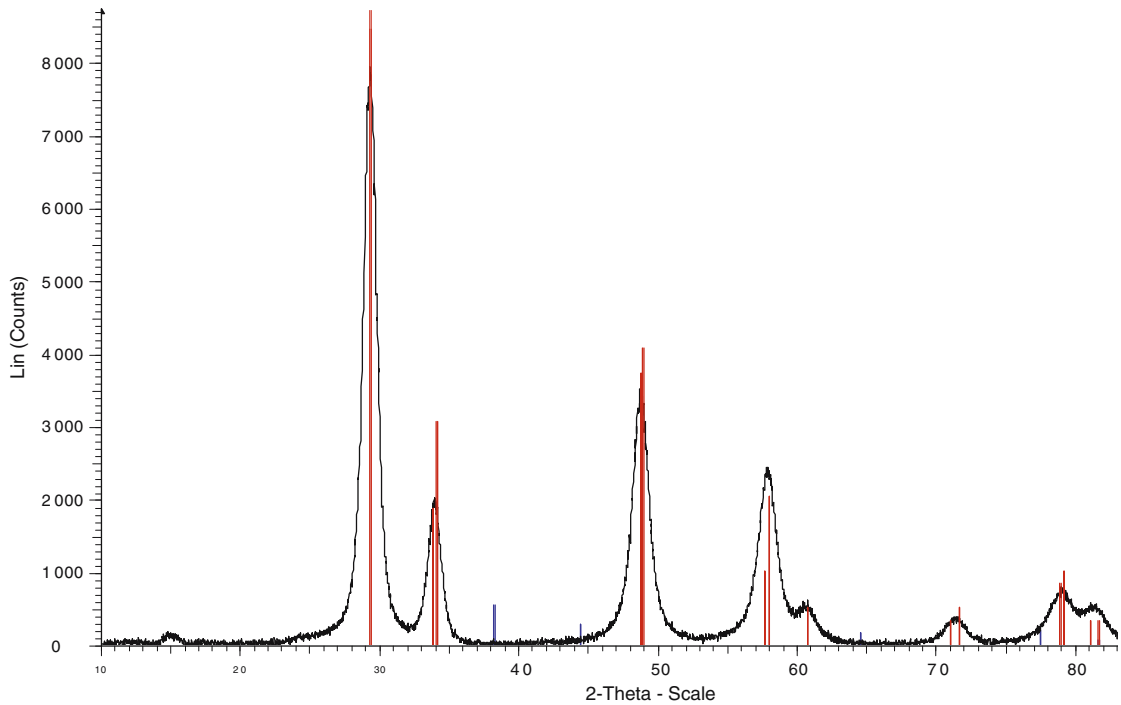

Figure 5. XRD of the as prepared 1.70 wt%$Au/CeZrO_4$ catalyst. The red and blue stick lines represent the diffraction lines of tetragonal $Ce_{0.5}Zr_{0.5}O_2$ (PDF 38-1436) and cubic Au (PDF 04-0784).

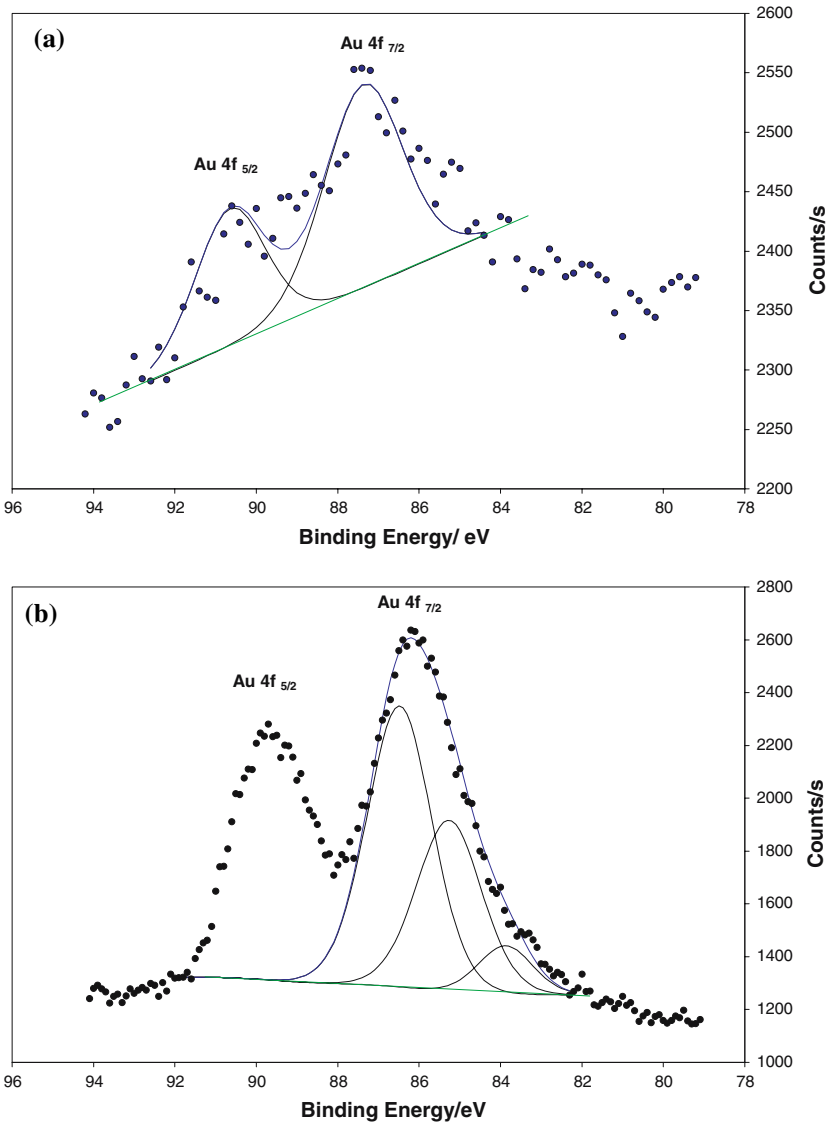

Figure 6. Au $4f_{7/2}$ XP spectra of the as-prepared (**a**) 0.19 and (**b**) 1.70 wt% $Au/CeZrO_4$ catalysts. For (**a**) the Au $4f_{7/2}$ and $4f_{5/2}$ profiles have been peak profiled and for (**b**) the $4f_{7/2}$ peak deconvoluted to reveal the individual components.

Figure 8c shows the same region after 6 min exposure, showing two features with at least twice as expected intensity.

We believe that the most likely explanation for these 0.3 nm features is that they are individual Au atoms that are highly mobile under the electron beam. However, without any supporting spectroscopic evidence to determine whether these features contain Au, this conclusion remains speculative.

The XP spectra and STEM images can be compared to the previously published Au L_{III} X-ray Absorption spectra (XAS) on the as-prepared 0.19 and 1.70 wt% Au catalysts [28]. X-ray Absorption Near-edge Spectra (XANES) of both catalysts showed sharp white line

Table 1
Summary of XPS Au $4f_{7/2}$ peak analysis of $Au/CeZrO_4$ catalysts

Au loading/wt%	$\%Au^0$		$4f_{7/2}$ BE/eV	$\%Au^+$		$4f_{7/2}$ BE/eV	$\%Au^{3+}$		$4f_{7/2}$ BE/eV
	At%	% of Au present		At%	% of Au present		At%	% of Au present	
0.19							0.13	100	87.3
0.87				0.45	35	85.4	0.83	65	86.7
1.70	0.21	8	83.9	0.91	35	85.3	1.49	57	86.5

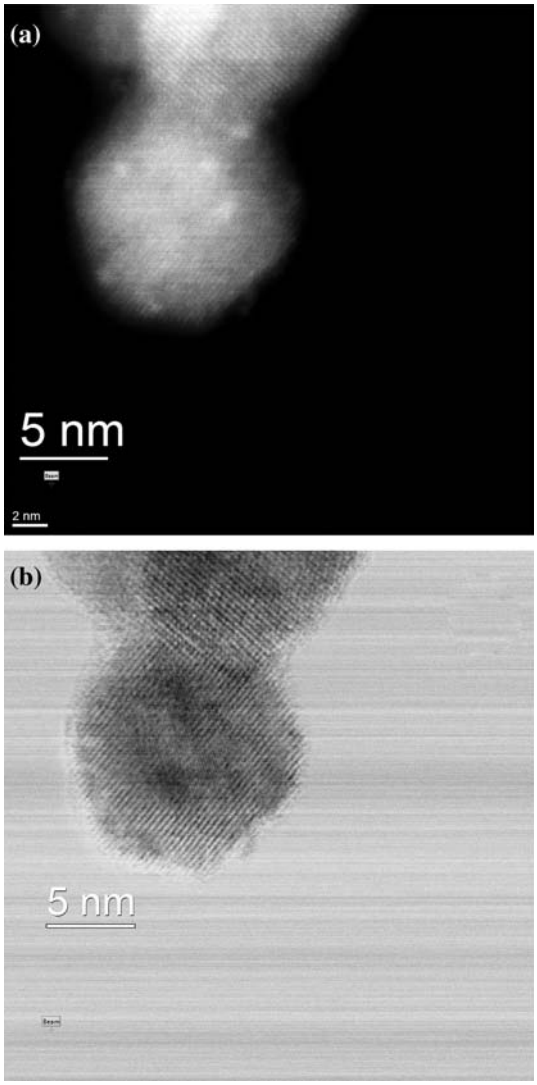

Figure 7. SuperSTEM images of the same region of the 1.70%Au/$CeZrO_4$ catalyst. (**a**) HAADF STEM image (**b**) Bright field STEM.

intensities indicating a high proportion of Au^{3+} present. Extended X-ray Absorption Fine Structure (EXAFS) spectra of the 1.70 wt% Au catalyst could be fitted to a first shell coordination of 3.6 ± 1.0 of O atoms at a distance of 0.198 ± 0.010 nm and a second shell coordination of 4.0 ± 1.0 of Ce ions at a distance of 0.335 ± 0.010 nm.

Combining this data suggests that the as-prepared (i.e. pre-tested) 0.19% Au catalyst contain primarily Au dispersed monotomically over the $CeZrO_4$ support as isolated Au^{3+} ions in 4 coordinate geometry with O near-neighbours. Recent Density Functional Theory (DFT) calculations of Au-CeO_2 low index surfaces suggest that the most stable configuration is Au sitting in a Ce vacancy site with a Au-O bond distance of 0.233 nm (Ce(111)) and 0.211 nm (Ce(110)) similar to the 0.198 nm found from the EXAFS experiments [24]. On increasing Au loadings as shown by STEM, an increasing proportion of the Au present is as small (< 2 nm) nanoparticles. This represents the Au speciation in the *as-prepared* catalysts and is not necessarily the active species responsible for the high WGS activity (see below). However, given that the lowest loaded Au catalyst shows the highest intrinsic tof for WGS and shows exclusively only Au^{3+} in the as-prepared state, it suggests that monodispersed Au ions are the best *precursor* state to give the highest activity Au/$CeZrO_4$ catalysts under WGS reaction conditions [40].

The XAS has also been used to study the 0.19 and 1.70wt% Au catalysts to determine the Au speciation under WGS conditions [28]. Interestingly, on passing a full WGS feed (2.0% CO, 2.5% CO_2, 7.5% H_2O, 8.1% H_2, balance N_2) over the catalysts at 100°C XANES showed a reduction to Au^0 with EXAFS of the 1.70 wt% Au catalyst showing only Au–Au distances (0.276 and 0.380 nm) with a coordination number of 6.6 ± 1.0 suggesting a particle size of *c.* 1 nm. Increasing the reaction temperature did not change the XANES or EXAFS parameters significantly. Therefore, under WGS reaction conditions the Au speciation is exclusively Au^0 and the Au^{3+} present in the as-prepared catalysts has been reduced.

3.4. TPR/Isothermal re-oxidations with H_2O

Figure 9 shows the WGS activity of 1.70 wt%Au and a 4.0 wt%Pt supported on $CeZrO_4$. The Au catalyst shows a clear 60–80 °C advantage in CO conversion. To understand why Au shows better effectiveness for WGS when supported on $CeZrO_4$ than Pt, a series of temperature programmed reductions and iso-thermal H_2O re-oxidations were performed.

Hydrogen temperature programme reductions (H_2-TPR) were performed on $CeZrO_4$, Au/$CeZrO_4$ and Pt/$CeZrO_4$ and the uptake profiles for $CeZrO_4$ and Au/$CeZrO_4$ are shown in figure 10. Uncatalysed $CeZrO_4$ shows a broad reduction peak with a maximum at 500 °C corresponding to the reduction of both surface and bulk Ce^{4+} to Ce^{3+}. The H_2 uptake was found to be 1.05 mmol H_2 g^{-1}, representing 62% reduction of Ce assuming all Ce was present as Ce^{4+}. The addition of Au lowers this reduction process to 109 °C with no further reduction below 800 °C. Interestingly, the H_2 uptake was found to be 0.63 mmol H_2 g^{-1}, representing only 37% of Ce present. The addition of Pt showed a similar shift in reduction temperature (90 °C), with a H_2 uptake of 1.70 mmol H_2 g^{-1}, representing 100% of Ce.

The degree of surface vs bulk reduction can be roughly estimated. Given a surface area of 100 m^2 g^{-1} and an effective Ce^{4+} ion area of 2.9×10^{-19} m^2, the $CeZrO_4$ will contain *c.* 3.5×10^{20} surface Ce ions (0.6 mmol Ce g^{-1}) assuming 50% surface occupancy. Since $CeZrO_4$ contains a total of 3.4 mmol of Ce, this gives a Ce surface to total ratio of *c.* 20%. This calculation suggests that although both Au and Pt are similar

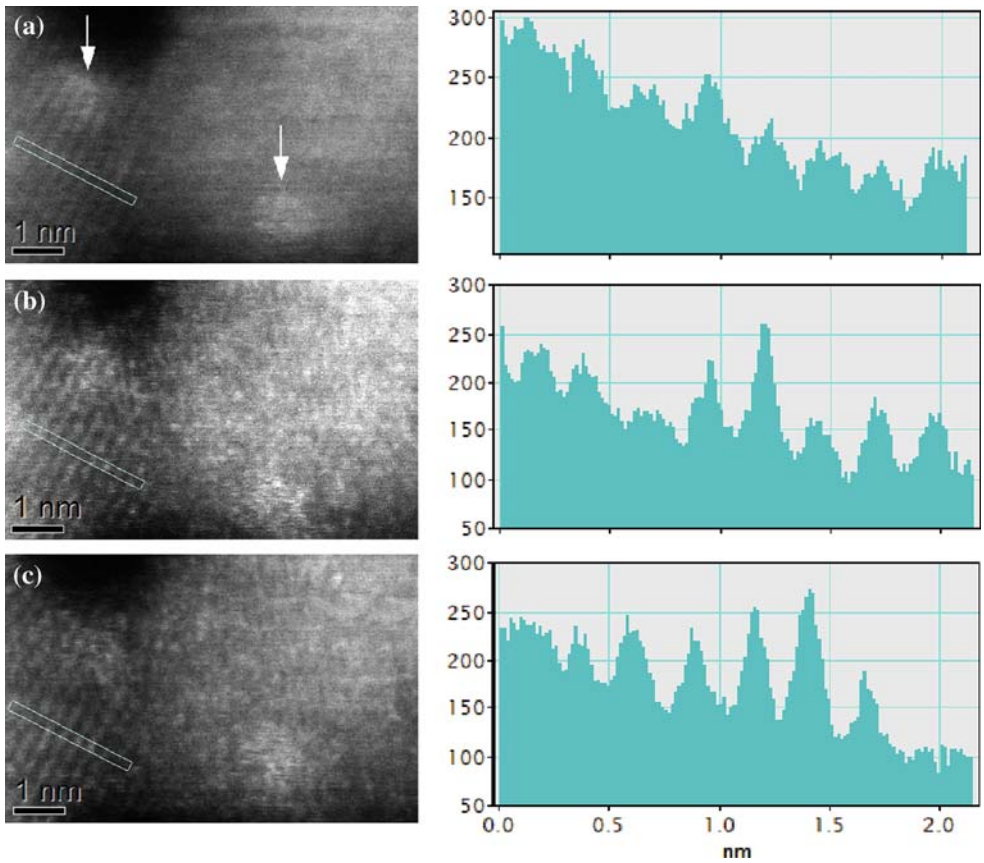

Figure 8. High-resolution SuperSTEM HAADF images of 1.70 wt% $CeZrO_4$ catalyst. Images (**a**), (**b**) and (**c**) represent a time sequence of 0, 3 and 6 min. To the right of each image are intensity line profiles across the same region of sample as indicated by the dotted rectangles in each HAADF image. High intensity features (*c*. 0.3 nm) appear in the line profiles of (**b**) and (**c**) and are mobile under extended beam exposure. Larger features (*c*. 1 nm) are arrowed in (**a**).

in their ability to promote Ce reduction, Pt is more effective in reducing both surface and bulk Ce^{4+}. In fact, Au only appears to reduce surface and near-surface Ce^{4+} and inhibit any further bulk reduction with H_2, perhaps due to the inability to adsorb H_2 when reduced. The ability of Au to promote reduction of CeO_2 is well known [41,42] and recently it has been shown that although Au shows similar shifts in reduction temperature of CeO_2 as Pt, it is less effective in the degree of reduction of the Ce [26,43].

The 3 samples were also reduced using CO TPR. Similar trends in reduction were observed to H_2-TPR, although CO appeared to be a poorer reductant compared to H_2. The bare $CeZrO_4$ was reduced in 2 stages

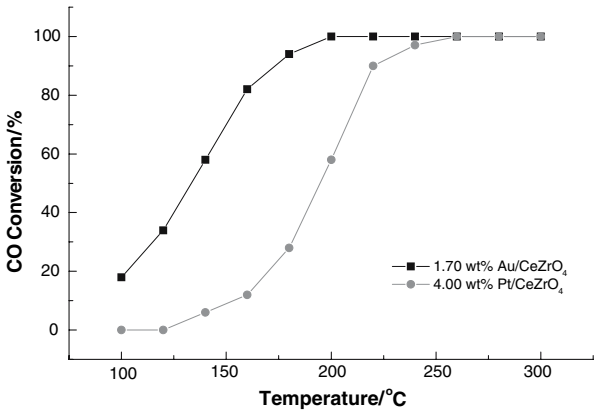

Figure 9. WGS activity (CO conversion) of 1.70 wt%Au and 4 wt%Pt/$CeZrO_4$ catalysts (5% CO, 30% H_2O, 65% N_2, 40,000 $cm^3g^{-1}h^{-1}$).

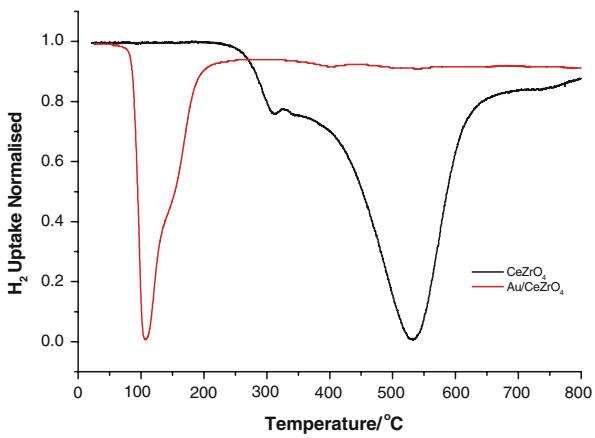

Figure 10. H_2-TPR profiles of $CeZrO_4$ and 1.70 wt% Au/$CeZrO_4$.

firstly at 300 °C and finally at 530 °C with a total CO uptake of 0.62 mmol g^{-1}. The amount of CO_2 found to be evolved during this reduction was also 0.62 mmol g^{-1}, indicating reduction of Ce^{4+} to Ce^{3+} and the formation of 0.5 CO_2 molecules per Ce^{4+} site. The CO/CO_2 uptake/release values indicate that both surface and bulk Ce^{4+} ions are being reduced. Both Au and Pt supported samples show shifts in reduction temperature to 80 and 70 °C, respectively. The Au sample showed a lower CO uptake (0.61 mmol CO g^{-1}) than Pt (1.1 mmol CO g^{-1}) again showing Au's inability to promote significant bulk Ce^{4+} reduction. Interestingly, for both the Au and Pt samples incomplete release of CO_2 was observed on reduction, indicating some retention of C–O species (figure 11).

The ability of H_2O to oxidise the H_2 reduced samples was investigated. The pre-reduced bare $CeZrO_4$ was found to be difficult to re-oxidise with H_2O, with only low amounts of H_2 released above 500°C. In contrast, Au and Pt were found to promote the re-oxidation at low temperatures (figure 12). Firstly, the Au/$CeZrO_4$ sample was reduced with H_2/N_2 to 200 °C consuming 0.63 mmol H_2 g^{-1}. Keeping isothermal at 200 °C, H_2O/N_2 was introduced and H_2 was released as the sample was oxidised with 0.38 mmol H g^{-1} released. The sample was then cooled to ambient and re-reduced to 200 °C, consuming 0.4 mmol H_2 g^{-1}. The sample was then heated to 350 °C in N_2 and H_2O/N_2 introduced releasing 0.68 mmol H_2 g^{-1}. This showed that all the reduced Ce could be re-oxidised by 350 °C by H_2O. The same H_2 TPR/iso-thermal H_2O experiment was performed on the Pt/$CeZrO_4$ sample. Although, by 200°C 1.7 mmol H_2 g^{-1} had been consumed, re-oxidation at 200 °C only released 0.13 mmol H_2 g^{-1}. Increasing the temperature to 350 °C released at total of 0.54 mmol H_2 g^{-1}, this represented only 55% of all the reduced Ce re-oxidised. Therefore, although Pt is more effective in reducing the bulk Ce at low temperatures, Au shows much higher activity in activating H_2O to oxidise reduced Ce thus releasing H_2.

The isothermal experiment was repeated with the 1.70 wt% Au/$CeZrO_4$ sample using CO as a reductant at 220 °C and cycled between CO and H_2O treatments. On treatment of CO, both CO_2 and H_2 were found to be released, with incomplete CO_2 release as found with the CO TPR experiment. Following an N_2 purge, H_2O was introduced isothermally and both H_2 and CO_2 were released. The cycle was repeated a number of times and the responses were found to be reproducible. The experiments suggest that carboneous species are formed by CO adsorption onto the catalyst under reducing conditions which are then decomposed on contact with H_2O, similarly to that found with Au/Fe_2O_3 and Au/CeO_2 [26,44]

Comparing the differences in WGS activity of the Au and Pt/$CeZrO_4$ catalysts with the differences in H_2 TPR and H_2O re-oxidation profiles show a clear correlation in WGS activity and the temperature of the oxidation of reduced catalysts by H_2O. Therefore, the lower onset temperature of WGS activity shown by Au/$CeZrO_4$ appear related to Au's ability to activate H_2O to oxidise reduced Ce sites to generate H_2. This would suggest that the low temperature WGS activity shown by Au and Pt catalysts is governed by the 'regenerative' mechanism. However, the use of CO as the reductant rather than H_2 shows evidence of both 'regenerative' and 'associative' reaction channels as shown by the retention of carbonaceous species on CO reduction and the release of CO_2 on re-oxidation with H_2O (tables 2, 3, 4).

3.5. Stability Studies

The stability of WGS activity of the 1.70 wt%Au/$CeZrO_4$ catalyst was studied as a function of both temperature ramp and steady-state exposure to WGS reactant streams. Figure 13 shows the WGS activity of the as-prepared Au/$CeZrO_4$ catalyst as shown previously. The temperature ramp was continued to 500°C under the CO/H_2O feed, cooled to ambient and re-tested. The resulting WGS activity was found to have reduced significantly with temperatures for similar %CO conversions increased by 70 °C. Repeated ramps to 500 °C gave stable but similar lower activity.

Table 2
H_2-TPR peak analysis of $CeZrO_4$, Au/$CeZrO_4$ and Pt/$CeZrO_4$

Sample	H_2 uptake/ mmol g^{-1}	Peak Temperature/ °C	Ce^{4+} (Ce^{3+} reduction/%
$CeZrO_4$	1.05	500	62
Au/$CeZrO_4$	0.63	105	37
Pt/$CeZrO_4$	1.70	92	100

Note: H_2 uptakes integrated between 25 and 900 °C for $CeZrO_4$, 25 and 200 °C for Au & Pt/$CeZrO_4$.

Table 3
CO-TPR peak analysis of $CeZrO_4$, Au/$CeZrO_4$ and Pt/$CeZrO_4$

Sample	CO uptake/ mmol g^{-1}	CO_2 release/ mmol g^{-1}	Peak reduction temperature/°C	Ce^{4+} reduction/%
$CeZrO_4$	0.62	0.62	520	37
Au/$CeZrO_4$	0.61	0.38	70–90	36
Pt/$CeZrO_4$	1.10	0.62	70	65

Table 4
H_2O re-oxidation peak analysis after H_2-TPR at 200 °C

Catalyst	H_2 release at 200°C/ mmol g^{-1}	Degree of total Ce oxidation/%	H_2 release at 350°C/ mmol g^{-1}	Degree of total Ce oxidation/%
Au/$CeZrO_4$	0.38	22	0.68	40
Pt/$CeZrO_4$	0.13	8	0.54	32

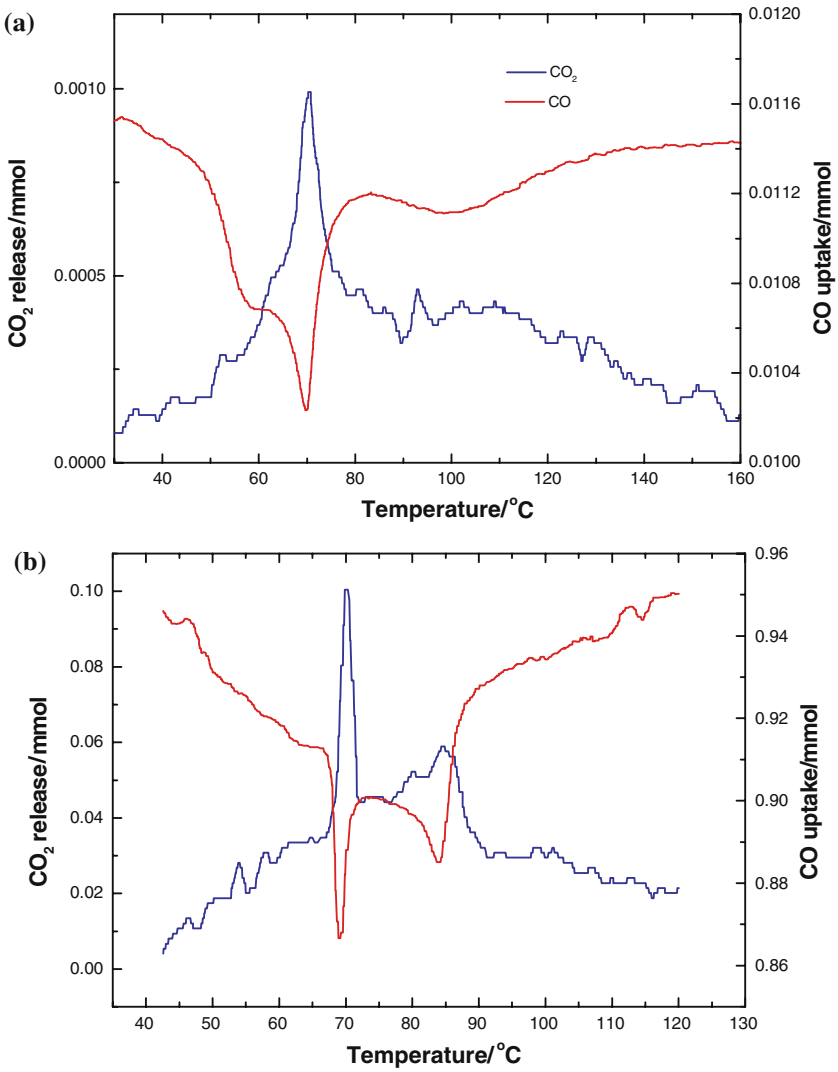

Figure 11. CO-TPR profiles of (a) $Pt/CeZrO_4$ and (b) $Au/CeZrO_4$.

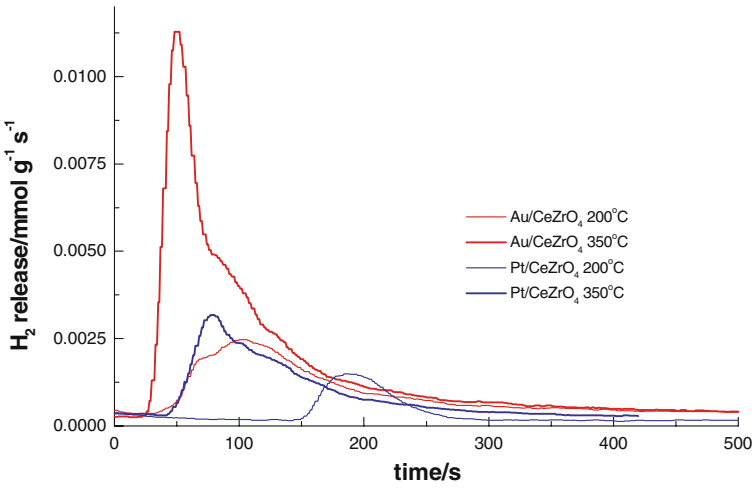

Figure 12. Comparison of $Au/CeZrO_4$ and $Pt/CeZrO_4$ re-oxidation with H_2O at 200 and 350 °C after pre-reduction with H_2 at 200 °C.

The Au catalyst was also treated under steady-state conditions under a full WGS feed (40%H_2, 10%CO, 10%H_2O, 40%N_2) at both 200 and 300 °C for 50 h and then retested under the simplified WGS conditions. The catalyst treated at 200 °C shows some modest deactivation (c. 20 °C) compared to fresh, however, the

300 °C treated sample showed the greatest deactivation of the 3 samples (80 °C).

The as-prepared and 500 °C treated samples were characterised using XPS and conventional TEM. As discussed previously, the XPS of the as-prepared Au catalyst showed predominately Au^{3+} character with some 'Au^{+}' and Au metal. After, treatment at 500 °C, only Au metal was observed (Au $4f_{7/2}$ B.E. 84.6 eV). HAADF images of the as-prepared catalyst showed no evidence of Au particles at the maximum resolution of this instrument. However, after the 500 °C treatment, the HAADF images show the presence of 2–3 nm Au particles amongst the larger $CeZrO_4$ particles (figure 14). Combining the XPS and TEM data suggests that the thermal treatment has caused modest sintering of the Au to give reduced Au particles of 2–3 nm.

These results can be compared to the previously reported *in-situ* EXAFS results on the 1.70 wt% Au/$CeZrO_4$ catalyst [28]. As discussed previously on exposing the as-prepared catalyst to a full WGS feed at 100 °C reduction of the Au resulting forming clusters with a first shell coordination number of 6.6 ± 1.0 indicating a particle size of between 0.9 and 1.3 nm depending on particle morphology. On heating the catalyst in the WGS feed to 350 °C significant loss in WGS activity was observed, however, the EXAFS analysis showed no change in Au first shell coordination (6.0 ± 1.0). The first shell coordination remained between 6 and 7 even after heating the catalyst to 450 °C with the WGS feed. Therefore, it was concluded that the deactivation in WGS activity was not due to gross Au particle sintering. Given the importance of Au–oxide interface sites in many mechanistic schemes, it was proposed that the deactivation was caused by 'de-wetting' of the support by the Au particles without change in the Au cluster size, thus reducing the number of direct Au interface sites necessary to mediate reaction, whether due to the regenerative or associative mechanistic pathways.

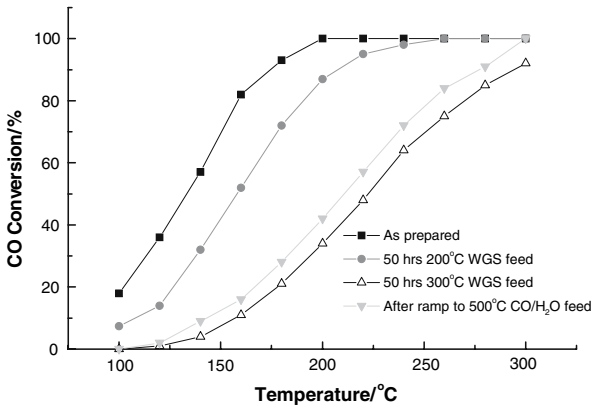

Figure 13. WGS activity (CO conversion) of 1.70 wt%Au/$CeZrO_4$ as-prepared, after WGS feed treatment at 200 °C, WGS feed treatment at 300 °C and after ramping to 500 °C with the simplified WGS feed (5%CO, 30%H_2O, 65%N_2).

Combining the two ageing studies on the 1.70 wt% Au/$CeZrO_4$ shows that on treatment with WGS feeds at low temperatures (< 200 °C), only reduced Au species are observed. EXAFS would suggest that these are small (*c.* 1 nm) Au clusters with good interaction with the $CeZrO_4$ support. These particles give the highest activity. On increasing reaction or ageing temperature (> 200 °C), activity decreases without any significant loss in Au cluster size but with a decrease in support interaction. At higher temperatures (> 450 °C), modest sintering of the Au clusters occurs giving 2–3 nm Au particles.

4. Conclusions

We have shown that Au supported on a $CeZrO_4$ support prepared by a modified deposition-precipitation route has higher activity for the water-gas shift reaction using a model reaction gas mixture than Au supported on CeO_2, TiO_2, ZrO_2 prepared in a similar manner and Au/'FeO(OH)' prepared by co-precipitation. Significant WGS activity was found at temperatures as low as 100 °C. A study of Au loading showed that the lowest loading (0.19 wt%) prepared gave the highest specific reaction rate and this rate dropped steadily as the loading was increased to 3 wt%. Characterisation of the as-prepared catalysts showed the 0.19 wt% catalyst consisted of only isolated Au^{3+} species. On increasing the Au loading, a high proportion of Au^{3+} species persisted together with an increase in Au cluster formation. Although, previous work had shown that only Au^0 clusters exist under WGS operating conditions, it is proposed that *as-prepared* (i.e. pre-tested) catalysts with a maximum proportion of isolated Au^{3+} species represents the ideal *precursor* state for reduction into the active species that give maximum catalytic activity under reaction conditions.

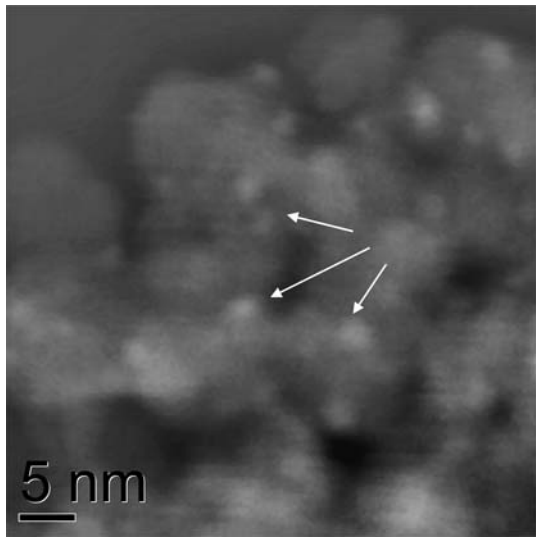

Figure 14. TEM HAADF image of 1.70 wt%Au/$CeZrO_4$ catalyst after treatment to 500 °C in model WGS feed. Au particles arrowed.

The origin of the low temperature activity of Au/$CeZrO_4$ with respect to Pt/$CeZrO_4$ was investigated using combined TPR and steady-state H_2O re-oxidation. Both H_2 and CO TPR showed little difference in the ability of Au and Pt to promote the reduction of $CeZrO_4$ in terms of temperature, although it was found Au only promoted surface and near-surface reduction of the $CeZrO_4$, while Pt promoted both surface and bulk reduction. However, following reduction, Au was found to more effective at promoting H_2O activation in terms of H_2 release at lower temperatures than Pt. It was proposed that this effect is the origin of the lower onset temperature shown by Au/$CeZrO_4$ compared to Pt/$CeZrO_4$.

The stability of the Au/$CeZrO_4$ catalyst was studied both by extended temperature ramps under model WGS conditions and *ex-situ* steady state ageing with a realistic WGS feed. Both approaches resulted in deactivation of the catalyst. Characterisation of the resulting catalysts showed evidence of increased Au particle formation.

Acknowledgments

We would like to thank the CenTACat group at Queen's University Belfast (Robbie Burch, Chris Hardacre, John Breen, Frederic Meunier, Daniele Tibiletti, Alex Goguet) for the XANES/EXAFS studies together with many stimulating discussions. Tony Busby for the XPS studies. The World Gold Council for part funding the work and in particular Richard Holiday and David Thompson for their interest and enthusiasm.

References

[1] A. Faur Ghenciu, Curr. Opin. Solid State Mater. Sci. 6 (2002) 389.
[2] D.P. Wilkinson and D. Thompsett, , Pages 224– in: *Materials and Approaches for CO and CO2 Tolerance for Polymer Electrolyte Membrane Fuel Cells, 32767 BC*, O. Savadogo and P.R. Roberge (eds.), (Ecole Polytechnique de Montreal, Montreal, 1997) pp. 224–.
[3] S.C. Ball and D. Thompsett, Ultra CO tolerant PtMo/PtRu anodes for PEMFCs Material Research Society Symposium Proceedings (2003), 756 (Solid State Ionics-2002), 353–364.
[4] J. Zhang, Z. Xie, J. Zhang, Y. Tang, C. Song, T. Navessin, Z. Shi, D. Song, H. Wong, D.P. Wilkinson, Z-S. Liu and S. Holdcroft, J. Power Sour. 160 (2006) 872.
[5] Q. Li, R. He, J.O. Jensen and N.J. Bjerrum, Chem. Mater. 15 (2003) 4896.
[6] W. Ruettinger, O. Olinich and R.J. Farrauto, J. Power Sour. 118 (2003) 61.
[7] D. Andreeva, V. Idakiev, T. Tabakova and A. Andreev, J. Catal. 158 (1996) 354.
[8] D. Andreeva, Gold Bull. 35/3 (2002) 82.
[9] A. Venugopal and M.S. Scurrell, Appl. Catal. A 258 (2004) 241.
[10] H. Sakurai, A. Ueda, T. Kobayashi and M. Haruta, Chem. Commun. (1997) 271.
[11] H. Sakurai and M. Haruta, Appl. Catal. A 127 (1995) 93.
[12] F. Boccuzzi, A. Chiorino, M. Manzoli, D. Andreeva, T. Tabakova, L. Ilieva and V. Iadakiev, Catal. Today 75 (2002) 169.
[13] V. Idakiev, T. Tabakova, Z.-Y. Yuan and B.-L. Su, Appl. Catal. A 270 (2004) 135.
[14] V. Idakiev, Z.-Y. Yuan, T. Tabakova and B.-L. Su, Appl. Catal. A 281 (2005) 149.
[15] T. Tabakova, V. Idakiev, D. Andreeva and L. Mitov, Appl. Catal. A 202 (2000) 91.
[16] V. Idakiev, T. Tabakova, A. Naydenov, Z.-Y. Yuan and B.-L. Su, Appl. Catal. B 63 (2006) 178.
[17] M.M. Mohamed, T.M. Salama and M. Ishikawa, J.Colloid Interface Sci. 224 (2000) 366.
[18] Q. Fu, A. Weber and M. Flytzani-Stephanopoulos, Catal. Lett. 77 (2001) 87.
[19] D. Andreeva, V. Idakiev, T. Tabakova, L. Llieva, P. Falanes, A. Bourlinos and A. Trovlos, Catal. Today 72 (2002) 9.
[20] Q. Fu, H. Saltsburg and M. Flytani-Stephanopoulos, Science 301 (2003) 935.
[21] Q. Fu, S. Kudriavtseva, H. Saltsburg and M. Flytzani-Stephanopoulos, Chem. Eng. J. 93 (2003) 41.
[22] Q. Fu, W. Deng, H. Saltsburg and M. Flytzani-Stephanopoulos, Appl. Catal. B 56 (2005) 57.
[23] J.M. Fisher, D. Thompsett, R.I. Walton and C.S. Wright, WO Patent 2006/030179 23 March 2006.
[24] C.H. Kim and L.T. Thompson, J. Catal. 244 (2006) 248.
[25] X. Wang, J.A. Rodriguez, J.C. Hanson, M. Pérez and J. Evans, J. Chem. Phys. 123 (2005) 221101.
[26] G. Jacobs, P.M. Patterson, L. Williams, E. Chenu, D. Sparks, G. Thomas and B.H. Davies, Appl. Catal. A 262 (2004) 177.
[27] R. Leppelt, B. Schumacher, V. Plzak, M. Kinne and R.J. Behm, J. Catal. 244 (2006) 137.
[28] D. Tibiletti, A. Amieiro-Fonseca, R. Burch, Y. Chen, J.M. Fisher, A. Goguet, C. Hardacre, P. Hu and D. Thompsett, J. Phys. Chem. B 109 (2005) 22553.
[29] D. Tibiletti, A. Goguet, D. Reid, F.C. Meunier and R. Burch, Catal. Today 113 (2006) 94.
[30] B. Aeijelts Averink Siberova, G. Mul, M. Makkee and J.A. Moulijn, J. Catal. 243 (2006) 171.
[31] R. Burch, Phys. Chem. Chem. Phys. 8 (2006) 5483.
[32] J. Kašpar and P. Fornasiero, in: *Catalysis by Ceria and Related Materials*, Vol 2, ed. A. Trovarelli (Imperial College Press, London, 2002) ch. 6, pp 217–242.
[33] D. Duprez & C. Descorme, in: *Catalysis by Ceria and Related Materials*, Vol 2, ed. A. Trovarelli (Imperial College Press, London, 2002) ch. pp 243–280.
[34] A. Wolf and F. Schűth, Appl. Catal. A 226 (2002) 1.
[35] J.J. Pireaux, M. Liehr, P.A. Thiry, J.P. Delrue and R. Caudano, Surf. Sci. 141 (1984) 221.
[36] S. Zafeiratos and S. Kennou, Surf. Sci. 443 (1999) 238.
[37] D. Dalacu, J.E. Klemberg-Sapieha and L. Martinu, Surf. Sci. 472 (2001) 33.
[38] E.A. Willneft, S. Braun, D. Rosenthal, H. Bluhm, M. Hävecker, E. Kleimenov, A. Knop-Gericke, R. Schlögl and S.L.M. Schroeder, J. Am. Chem. Soc. 128 (2006) 12052.
[39] D. Boyd, S. Golunski, G.R. Hearne, T. Magadzu, K. Mallick, M.C. Raphulu, A. Venugopal and M.S. Scurrell, Appli. Catal. A 292 (2005) 76.
[40] A. Amieiro-Fonseca, J.M. Fisher & D.Thompsett, WO Patent 2005/087656 22 Sept 2005.
[41] R.R. Rajaram, J.W. Hayes, G.P. Ansell and H.A. Hatcher, EP Patent 0602865 22 June 1994.
[42] S. Golunski, R. Rajaram, N. Hodge, G.J. Hutchings and C.J. Kiely, Catal. Today 72 (2002) 107.
[43] G. Jacobs, E. Chenu, P.M. Patterson, L. Williams, D. Sparks, G. Thomas and B.H. Davis, Appl. Catal. A 258 (2004) 203.
[44] C.H. Kim and L.T. Thompson, J. Catal. 230 (2005) 66.